Biomechanics and Modeling in Mechanobiology (2021) 20:2393–2412
https://doi.org/10.1007/s10237-021-01515-8

ORIGINAL PAPER

Significance of entropy generation and heat source: the case of peristaltic blood flow through a ciliated tube conveying Cu-Ag nanoparticles using Phan-Thien-Tanner model

Asgar Ali[1] · **R. N. Jana**[2] · **Sanatan Das**[3]

Received: 6 April 2021 / Accepted: 18 August 2021 / Published online: 29 August 2021
© The Author(s), under exclusive licence to Springer-Verlag GmbH Germany, part of Springer Nature 2021

Abstract

The present speculative investigation is concentrated to analyze the entropy generation and heat transfer phenomena in ciliary induced peristalsis of blood with the suspension of hybrid nanoparticles in a tube with heat source impact. The blood is assumed to contain copper (Cu) and silver (Ag) nanoparticles (NPs). The ciliary inner wall of the tube has been considered with small hair-like structures. The Phan-Thien-Tanner (PTT) fluid model is employed to describe the non-Newtonian rheological characteristics of blood. The conservative equations are normalized and simplified by utilizing scaling analysis with the assumption of low Reynolds number and large wavelength approximations. The analytical inspection exposes that the total entropy generation gets a decrement for mounting values of cilia length, while reversed impact is detected for an increment in heat source parameter. Hybrid nano-blood exhibits a greater total entropy number than mono nano-blood. This research study may be beneficial to medical experts and researchers in the field of embryology. Cysts in the ciliated fallopian tube, where embryos develop, are removed by using nanoparticles (nano-drug delivery).

Keywords Phan-Thien-Tanner (PTT) model · Peristaltic flow · Hybrid nano-blood · Entropy generation (EG) · Heat source · Ciliated tube

List of symbols

$\tilde{a}$	Mean radius of tube
Be	Bejan number
Br	Brinkman number
c	Metachronal wave speed
C_{p}	Specific heat
E_{g}	Characteristic entropy generation rate
F	Mean flow rate
h	Ciliated wall
k	Thermal conductivity
N_{S}	Non-dimensional entropy generation rate
$\tilde{P}$	Pressure in the laboratory frame
p	Pressure in wave frame
Q	Volume flow rate
Q_0	Internal heat source coefficient
Re	Reynolds number
t	Non-dimensional time parameter
$\tilde{t}$	Dimensional time parameter
$\tilde{T}$	Blood temperature
$\tilde{T}_0$	Temperature at tube wall
(u, w)	Non-dimensional velocity components in (r, z)
$(\tilde{u}, \tilde{w})$	Moving frame velocity components in $(\tilde{r}, \tilde{z})$
$(\tilde{U}, \tilde{W})$	Fixed frame velocity components in $(\tilde{R}, \tilde{Z})$
We	Weissenberg number
$\tilde{Z}_0$	Reference particle position
Z^*	Heat transfer coefficient

Greek Symbols

α	Eccentricity due to elliptical movement
β	Wave number
δ	Dimensional cilia length
γ	Heat source parameter
λ	Metachronal wavelength
Λ	Relaxation time
μ	Constant viscosity coefficient
(ϕ_1, ϕ_2)	Solid Volume fractions of Cu and Ag-NPs
ψ	Stream function
ρ	Blood density

✉ Asgar Ali
asgaralimath@gmail.com

[1] Department of Mathematics, Bajkul Milani Mahavidyalaya, Purba Medinipur 721 655, India

[2] Department of Applied Mathematics, Vidyasagar University, Midnapore 721 102, India

[3] Department of Mathematics, University of Gour Banga, Malda 732 103, India

$\tilde{\tau}$	Extra stress tensor
τ_{ij}	Component of stress tensor
θ	Non-dimensional blood temperature
$\tilde{\theta}_0$	Temperature difference
ε	Elongation parameter
ζ	Temperature difference parameter

Subscript

s_1	Copper nanoparticles (Cu-NPs)
s_2	Silver nanoparticles (Ag-NPs)
f	Base fluid (blood)
nf	Cu-blood nanofluid
hnf	Cu-Ag/blood hybrid nanofluid

1 Introduction

In the 21st century, the phenomenon of peristalsis has become very exigent in the study of physiological transport mechanisms and biomedical industries. This mechanism appears mainly in living organs and organisms. In the peristaltic transport mechanism, physiological fluids are driven through confined tubes/channels/ducts by rhythmic continuous contraction/expansion of the adjacent materials. This mechanical process has an imperative role in medical, physiological, industrial, and engineering processes, for example, cilia movement, food bolus movement in stomach, blood circulation via arteries/ vessels, urine transport through ureters, chyme movement in gastrointestinal tract, sperm transport from male reproductive tract, motion of ovum in fallopian tube, liver, small intestine, and earthworm locomotion, etc. The peristaltic flow principle is adapted in many biomedical devices, for example, blood pump machine, heart-lung machine, ventilator machine, dialysis machine, insulin delivery, roller and finger pumps, stethoscope, glucose-sensing, etc. (Husband et al. 2004; Tamada et al. 2002). Latham (1966) first time reported the mechanism of peristalsis. After his pioneer study, the transport phenomena via peristalsis have been massively researched by numerous scholars under various physiological and geometrical aspects. Vajravelu et al. (2007) highlighted the thermal feature of peristaltic transport of viscous fluid through a tube via long-wave assumption. Akbar and Nadeem (2012) presented the simulation of non-Newtonian nanofluid in a diverging tube due to peristalsis. A mathematical model for the peristaltic transportation of blood containing nanoparticles through an artery with deformable wall was elucidated by Abdelsalam and Vafai (2017). Some other relevant examinations in this domain are provided in Refs. (Reddy and Makinde 2016; Makinde et al. 2017; Reddy et al. 2017; Mehmood et al. 2020; Vaidya et al. 2021a, b; Rajashekhar et al. 2021).

In the current era, bionanotechnology has radically changed the biomedical and engineering sciences. Cooling issues and product quality control in the shortest amount of time are two major challenges confronting manufacturing industries as heat production continues to rise. In order to save energy and reduce process time, scientists have come to appreciate the distinct nature and thermal properties of some fluids formed by incorporating micrometer or millimeter sized solid particles (Song et al. 2021). Recently, various novel nanomaterials were successfully developed by scientific community to utilize in biomedical, biomechanics, and bioengineering processes. Nanoparticles are metallic or non-metallic tiny-sized particles (10-100 nm) with augmented thermo-physical characteristics. Nanofluid (NF) was invented by Choi (1995) and found that the thermal characteristics of the working host fluid can be enhanced by the impulsion of nanoparticles into it. Due to vast applications of nanofluids in electrical, electronics, medical and modern sciences, many researchers (Das et al. 2020; Abo-Dahab et al. 2021; Ali et al. 2021) have extensively investigated the nanofluid flow with various aspects. In the biomedical domain, nanofluids are being massively administrated in pharmaceutical processes, wound treatment, resonance imaging, vivo therapy, surgeries, cancer tumor remedy, and nano cryosurgery, etc. Among various nanoparticles, copper (Cu) and silver (Ag) nanoparticles seem to have attracted the fewest interests in terms of their potential applications. Copper is a key component and a catalyst for many enzymes and proteins in the human body, so it can control human health via multiple mechanisms. Based on the biological functions, copper nanoparticles show unique properties in protecting the cardiovascular system, promoting bone fracture healing and antibacterial effects, Positron Emission Tomography (PET) imaging, promoting cure, killing cancer cells, and radio-immunological tracing and cancer radiotherapy (Wang et al. 2021). On another side, Ag-nanoparticles have ensured a rapid adoption in medical practice due to their unique physicochemical properties. Silver nanoparticles play an important role in the inhibiting/killing of numerous pathogenic-microorganisms (antimicrobial), biosensors, anti-diabetic agents, anticancer therapy, vaccine adjuvant, promoting of wound repair and bone healing (Hayat et al. 2017; Xu et al. 2020).

Hybrid nanofluids (HNFs) are an advanced generation of nanofluids that convey dissimilar nanomaterials in a host base fluid (Sarkar et al. 2015). These types of nanofluids have higher proficiency to augment thermo-physical properties as contrast to mono nanofluids. This new emergent class of nanofluids has enormous applications in all fields of sciences. In hemodynamics, blood is taken as the host liquid and can be treated as a suspension of hybrid nanoparticles. Various theoretical and experimental examinations available in literature explored that the incredible enhancement in the thermo-physical properties by using hybrid nanofluids. Ijaz and Nadeem (2018)

illustrated the transport of blood with the concentration of hybrid nanoparticles through a stenosed artery. Ijaz et al. (2018) developed a mathematical model for hybrid Cu-CuO nano-blood flow through an artery having stenosis. Sadaf et al. (2019) exposed the upshots of hybrid nanoparticles suspension in blood during the peristaltic pumping through an endoscope with wall properties. Their observation disclosed that the temperature in the blood flow is sharply dropped owing to the dispersion of hybrid nanoparticles in the blood. It is asserted in Sowmya et al. (2021) that increasing NPs volume fraction has a substantial impact on the thermal profile and streamlined of stagnant fluid flow. Significance of NPs volume fraction in nanofluid (Al_2O_3-water) flow over a uniformly thickened surface with heat source/sink, and Coriolis force has been presented by Oke et al. (2021). Their outcomes show that an increment in NPs volume fraction explores boosting behavior for local Nusselt number. Moreover, the adding of Al_2O_3 NPs can help to detect enhancements in hardness, strength and tensile strength of the Mg-matrix. Elnaqeeb et al. (2021) examined the insight into the flow dynamics of water-based nanofluids with three different nanoparticles of smaller and substantial large densities. They concluded that greater Nusselt numbers relative to heat transfer were detected in the case of water mixed with heavy densities nanomaterials (i.e., copper, copper oxide, and silver) at all expanding ratios and suction rates. In a research, Koriko et al. (2021) discovered that an increasing trend in buoyancy is reliable for increasing the velocity profiles for both fluids (Au-blood Carreau nanofluid and dusty fluid). Several significant studies on peristalsis dynamics of hybrid nanofluids are communicated in Refs. (Abdelsalam et al. 2020; Saleem et al. 2020; Ellahi et al. 2020; Shahzadi et al. 2020).

Rheological characteristics of the viscoelastic fluids like some condensed solute-solvent polymeric solutions and polymeric melts can be correctly predicted by the Phan-Thien-Tanner (PTT) model (Phan-Thien and Tanner 1977, 1978). Oliveira and Pinho (1999) analytically studied the viscoelastic fluids flow through channel/pipe via PPT fluid model and reported that the PPT model accomplishes lower shear stress compared to the upper-convective Maxwell (UCM) fluid/Newtonian fluid. In polymer processing industries, thermofluid characteristics of melted polymer flow in channel/pipes at high temperature are very important for efficient polymer processing equipment. Recently, the peristalsis flow of a Phan-Thien-Tanner fluid model has attracted the consciousness of researchers. El Naby (2009) examined the creeping PTT fluid flow through a peristaltic tube. Peristalsis flow of a PTT fluid inside a divergent tube has been explored by Akbar and Nadeem (2012). Some peristaltic flow models of PTT fluids through various flow regimes like a tube, channel, diverging/asymmetric tube/channel are reported in references (Hayat et al. 2012; Vajravelu et al. 2016, 2016).

Cilia-induced flow is significant in the locomotion of the cells themselves or other substances past the cell surface. Cilia can be explained as very tiny hair-resembling structures that transpire throughout the surface of eukaryotic cells and biological vessels. They behave like oars, whipping back and forth in unison to generate a wave pattern traveling along the surface, such wave is called metachronal wave. Moving cilia in the respiratory tract (Bustamante-Marin and Ostrowski 2017; Knowles and Boucher 2002) is accountable for assisting fluid flow on the cell surface by their beating movement to remove mucus and dust to clean off airways. In the digesting tract Pablo et al. (2016), cilia assists food and its egestation movement. Ciliated female fallopian tubes (Ghazal et al. 2014; Eddy and Pauerstein 1980) carry the egg and sperm through the oviducts. Cilia blends sperms in male efferent ductules (Lehti and Sironen 2017) to prevent them from aggregating and blockading the tube so they can transfer to their final destination. They are also observed in kidneys, ears, eye retina, and brain. Cilia finds its diverse applications in biomedicine, bioengineering, and physiological disciplines (Mills et al. 2012; Drummond 2012; Agrawal and Anawaruddin, 1984). Cilia plays as a sensory-antenna in our kidneys. They perceive signals from the nearby urine and transmit a response to alert the cells about the flow of it. Qiu et al. (2014) presented an interesting observation dealing with the movement of micro-organisms in non-Newtonian fluid induced by cilia and flagella. The mobility of cells in a viscous fluid induced by harmonic waves was investigated by Brennen (1974). Wu et al. (2020) studied the transportation of Carreau fluid due to ciliary motion. Farooq and Siddiqui (2017) performed a study on cilia-induced flow of a couple-stress fluid. Farooq et al. (2019) illustrated the peristaltic pumping of a micropolar fluid due to cilia beating through a tube.

In physiological structures, spontaneous chemical reactions take place by a drop in free-energy. In living organisms, for example, metabolism involving various chemical reactions generates free-energy and is associated with significant production of entropy. Anti-entropic functions such as dynamical flow of substances (sweat, urination, sperms, and blood flow, etc.), muscle contractions, and biosynthesis are usually considered as compensating for entropy in physiological systems. In recent years, the assessment of entropy generation (EG) during the flow of physiological fluids is of main concerned and challenging research field (Makinde 2012; Adesanya and Makinde 2015; Chamkha and Selimefendigil 2018; Butt et al. 2013) due to its crucial role in physiology, medicine, bioengineering, and biomechanics. Motivated by the pioneer work of Bejan (Bejan 1979, 1982) in this domain, many researchers (Marzougui et al. 2021; Fares et al. 2021) have

examined the entropy generation under various aspects. Souidi et al. (2009) assessed the entropy generation rate in the peristaltic flow of biological fluid. This work was elaborated by Akbar (2015) under the magnetic impact. Saleem (2018) and Munawar et al. (2016) have enquired about the entropy rate in peristaltic flow through symmetric/asymmetric channels with variable viscosity property. Later on, they (Saleem and Munawar 2020) researched entropy analysis in the ciliary flow of biomagnetic fluids. Abrar et al. (2020) analyzed the entropy generation in the flow of magneto-nanofluid through a ciliated tube with Joule heating. They concluded that the entropy production enhances due to larger concentration of nanoparticles. Recently, an analysis of entropy generation in cilia-induced peristaltic flow in the microchannel under the impact of magnetic field was elucidated by Munawar and Saleem (2020).

It is identified that no study is found in the literature, where the entropy generation and heat transport analysis in ciliary induced peristaltic motion of blood with non-Newtonian fluid model through a tube is deliberated under the concentration of hybrid nanoparticles. In view of this, our intention here to assess the entropy generation in the peristaltic transport of hybrid nano-blood (Cu-Ag/blood) with Phan-Thien-Tanner fluid model due to the metachronal beating of cilia through a tube. The constitutive equations are formulated in a cylindrical coordinate system and simplified by employing lubrication approximations. Exact solutions are achieved for the non-dimensional transformed equations. Numerical integration scheme is deployed to compute the pressure-rise per metachronal wavelength (MW) and frictional forces (FR) at the ciliated tube by using Mathematica built-in program. The physical impacts of various evolving parameters on the velocity profile, temperature profile, pressure gradient, pressure rise, heat transfer coefficient, streamlines, total entropy generation number, and Bejan number are illustrated graphically and interpreted in all physical aspects in the results and discussion section. The novelty of our current work is to explore a comprehensive insight into the peristaltic transport and thermal phenomena of non-Newtonian blood with the suspension of hybrid nanoparticles through a tube owing to metachronal wave-propulsion of the beating cilia. This examination will be more exposed by placing the following research questions:

- What is the role of entropy generation (EG) in hybrid nano-blood flow through ciliary tube?
- How heat source modify the entropy generation (EG) and temperature variation?
- What are the potential strategies for improving the thermal characteristics of a conventional fluid?
- What are the main drawbacks of mono nanofluids as a contrast to hybrid nanofluids?
- How the blood motion due to cilia beating is altered by the volumetric concentration of hybrid nanoparticles?

2 Mathematical formulation

Consider the two-dimensional laminar incompressible flow of a non-Newtonian hybrid nano-blood with Phan-Thien-Tanner (PTT) fluid model in a ciliated tube of length L. The flow is induced by the cilia beating. Blood is simulated as a homogeneous suspension with dispersed dissimilar (hybrid) nanoparticles (Cu-Ag NPs). A cylindrical coordinate system $(\tilde{R}, \tilde{\theta}, \tilde{Z})$ is considered to formulate the modeled problem, where $\tilde{R}$ is radial coordinate, $\tilde{\theta}$ the azimuthal coordinate, and $\tilde{Z}$ the axial coordinate. There is no flow in the azimuthal $(\tilde{\theta})$ direction due to the assumption of an axisymmetric blood flow in the ciliated tube. The wall of the ciliated tube is sustained with the uniform temperature T_0. Phan-Thien-Tanner (PTT) fluid model is engaged to mimic the non-Newtonian characteristics of blood. The constitutive relation for PTT fluid is given by (Phan-Thien and Tanner 1977, 1978):

$$\tilde{f}(tr(\tilde{\tau}))\tilde{\tau} + \Lambda\tilde{\tau}^{\Delta} = \mu_{hnf}(\nabla\mathbf{V} + (\nabla\mathbf{V})^{T}), \tag{1}$$

where

$$\tilde{\tau}^{\Delta} = \frac{\partial\tilde{\tau}}{\partial t} + \mathbf{V}\cdot\nabla\tilde{\tau} - \tilde{\tau}\cdot\nabla\mathbf{V} - (\nabla\mathbf{V})^{T}\cdot\tilde{\tau}, \tag{2}$$

$$\tilde{f}(tr(\tilde{\tau})) = 1 + \frac{\varepsilon\Lambda}{\mu_{hnf}}tr(\tilde{\tau}), \tag{3}$$

in which ε is a free parameter related to the extensional properties of the fluid, Λ the relaxation time, μ_{hnf} a constant viscosity coefficient, $\tilde{\tau}$ the extra stress tensor and $\tilde{\tau}^{\Delta}$ Oldroyd's upper convected derivative (Akbar and Nadeem 2012). The extensional parameter ε has a consequence on the shear properties as well as it imparts shear-thinning to the fluid provided that its value is not too small. The envelopes of the cilia tips can be expressed mathematically as (Blake 1971, 1972):

$$\tilde{R} = \tilde{H} = \tilde{F}(\tilde{Z}, \tilde{t}) = \tilde{a} + \delta\tilde{a}\cos\left(\frac{2\pi}{\lambda}(\tilde{Z} - c\tilde{t})\right), \tag{4}$$

$$\tilde{Z} = \tilde{G}(\tilde{Z}, \tilde{Z}_0, \tilde{t}) = \tilde{a} + \delta\tilde{a}\alpha\sin\left(\frac{2\pi}{\lambda}(\tilde{Z} - c\tilde{t})\right), \tag{5}$$

where $\tilde{a}$ designates the mean radius of the ciliated tube, δ the non-dimensional measure of the cilia length, λ the metachronal wavelength, c metachronal wave speed, $\tilde{Z}_0$ the reference particle position, and α the eccentricity due to elliptical movement. Physically, large number of cilia merge and exhibit a beating pattern on the inner wall of the tube.

This beating pattern generates a continuous chain of waves that acts like a peristaltic or sinusoidal wave at the wall of the tube. Eqs. (4–5) represent the geometry of cilia movement in the form of elliptical shape.

The velocity components of the blood flow induced by the cilia tips can be mathematically expressed as (Blake 1971, 1972) Fig. 1:

$$\tilde{W} = \left(\frac{\partial \tilde{Z}}{\partial \tilde{t}}\right)_{\tilde{Z}_0} = \frac{\partial \tilde{G}}{\partial \tilde{t}} + \frac{\partial \tilde{G}}{\partial \tilde{Z}}\frac{\partial \tilde{Z}}{\partial \tilde{t}} = \frac{\partial \tilde{G}}{\partial \tilde{t}} + \frac{\partial \tilde{G}}{\partial \tilde{Z}}\tilde{W} \tag{6}$$

$$\tilde{U} = \left(\frac{\partial \tilde{R}}{\partial \tilde{t}}\right)_{\tilde{Z}_0} = \frac{\partial \tilde{F}}{\partial \tilde{t}} + \frac{\partial \tilde{F}}{\partial \tilde{Z}}\frac{\partial \tilde{Z}}{\partial \tilde{t}} = \frac{\partial \tilde{F}}{\partial \tilde{t}} + \frac{\partial \tilde{F}}{\partial \tilde{Z}}\tilde{W} \tag{7}$$

In view of Eqs. (4–5), Eqs. (6–7) are rewritten as:

$$\tilde{W} = -\frac{\frac{2\pi}{\lambda}\delta\alpha\tilde{a}c\cos\left(\frac{2\pi}{\lambda}(\tilde{Z}-c\tilde{t})\right)}{1-\frac{2\pi}{\lambda}\delta\alpha\tilde{a}\cos\left(\frac{2\pi}{\lambda}(\tilde{Z}-c\tilde{t})\right)} \tag{8}$$

$$\tilde{U} = \frac{\frac{2\pi}{\lambda}\delta\alpha\tilde{a}c\sin\left(\frac{2\pi}{\lambda}(\tilde{Z}-c\tilde{t})\right)}{1-\frac{2\pi}{\lambda}\delta\alpha\tilde{a}\cos\left(\frac{2\pi}{\lambda}(\tilde{Z}-c\tilde{t})\right)} \tag{9}$$

The governing equations in the fixed frame (laboratory frame) for an incompressible viscoelastic PTT hybrid nanoblood flow are given by (Akbar and Nadeem 2012; Butt et al. 2020):

$$\frac{\partial \tilde{U}}{\partial \tilde{R}} + \frac{\tilde{U}}{\tilde{R}} + \frac{\partial \tilde{W}}{\partial \tilde{Z}} = 0, \tag{10}$$

$$\rho_{hnf}\left(\frac{\partial \tilde{U}}{\partial \tilde{t}} + \tilde{U}\frac{\partial \tilde{U}}{\partial \tilde{R}} + \tilde{W}\frac{\partial \tilde{U}}{\partial \tilde{Z}}\right) = -\frac{\partial \tilde{P}}{\partial \tilde{R}} - \frac{1}{\tilde{R}}\frac{\partial}{\partial \tilde{R}}(\tilde{R}\tilde{\tau}_{\tilde{R}\tilde{R}}) - \frac{\partial}{\partial \tilde{Z}}(\tilde{\tau}_{\tilde{R}\tilde{Z}}) - \frac{\tilde{\tau}_{\tilde{\theta}\tilde{\theta}}}{\tilde{R}}, \tag{11}$$

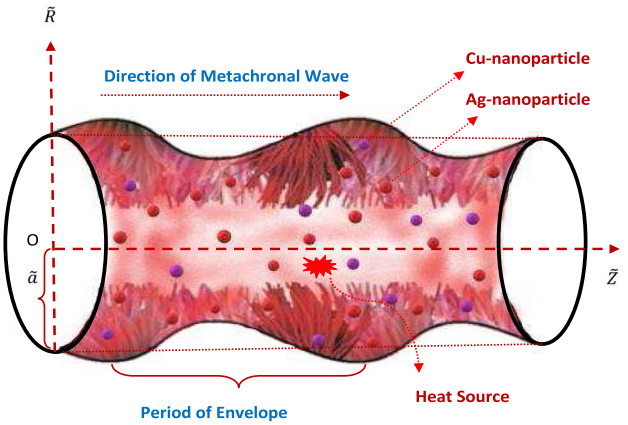

Fig. 1 Physical model of the problem

$$\rho_{hnf}\left(\frac{\partial \tilde{W}}{\partial \tilde{t}} + \tilde{U}\frac{\partial \tilde{W}}{\partial \tilde{R}} + \tilde{W}\frac{\partial \tilde{W}}{\partial \tilde{Z}}\right) = -\frac{\partial \tilde{P}}{\partial \tilde{Z}} + \frac{1}{\tilde{R}}\frac{\partial}{\partial \tilde{R}}(\tilde{R}\tilde{\tau}_{\tilde{R}\tilde{Z}}) + \frac{\partial}{\partial \tilde{Z}}(\tilde{\tau}_{\tilde{Z}\tilde{Z}}), \tag{12}$$

$$\begin{aligned}(\rho c_p)_{hnf}&\left(\frac{\partial \tilde{T}}{\partial \tilde{t}} + \tilde{U}\frac{\partial \tilde{T}}{\partial \tilde{R}} + \tilde{W}\frac{\partial \tilde{T}}{\partial \tilde{Z}}\right)\\ &= \tilde{\tau}_{\tilde{R}\tilde{R}}\frac{\partial \tilde{U}}{\partial \tilde{R}} + \tilde{\tau}_{\tilde{R}\tilde{Z}}\frac{\partial \tilde{W}}{\partial \tilde{R}} + \tilde{\tau}_{\tilde{Z}\tilde{R}}\frac{\partial \tilde{U}}{\partial \tilde{Z}} + \tilde{\tau}_{\tilde{Z}\tilde{Z}}\frac{\partial \tilde{W}}{\partial \tilde{Z}}\\ &\quad + k_{hnf}\left(\frac{\partial^2 \tilde{T}}{\partial \tilde{R}^2} + \frac{1}{\tilde{R}}\frac{\partial \tilde{T}}{\partial \tilde{R}} + \frac{\partial^2 \tilde{T}}{\partial \tilde{Z}^2}\right) + Q_0,\end{aligned} \tag{13}$$

where $\tilde{P}$ is the pressure, $\tilde{U}, \tilde{W}$ the respective velocity components in the radial $\tilde{R}$ and axial $\tilde{Z}$ directions in the fixed frame, $\tilde{T}$ the temperature, k_{hnf} the thermal conductivity of hybrid nanofluid, ρ_{hnf} the density of hybrid nanofluid, $(c_p)_{hnf}$ the specific heat of hybrid nanofluid at constant pressure, and Q_0 the internal heat source coefficient.

In the fixed (laboratory) frame, the suitable boundary conditions for the flow configuration are proposed as (Hanasoge et al. 2017):

$$\begin{aligned}&\frac{\partial \tilde{W}}{\partial \tilde{R}} = 0,\ \frac{\partial \tilde{T}}{\partial \tilde{R}} = 0,\ \text{at } \tilde{R} = 0,\\ &\tilde{W} = -\frac{\frac{2\pi}{\lambda}\delta\alpha\tilde{a}c\cos(\frac{2\pi}{\lambda}(\tilde{Z}-c\tilde{t}))}{1-\frac{2\pi}{\lambda}\delta\alpha\tilde{a}\cos(\frac{2\pi}{\lambda}(\tilde{Z}-c\tilde{t}))},\\ &\tilde{T} = \tilde{T}_0 \text{ at } \tilde{R} = \tilde{H} = \tilde{a} + \delta\tilde{a}\cos(\frac{2\pi}{\lambda}(\tilde{Z}-c\tilde{t})).\end{aligned} \tag{14}$$

In the fixed frame $(\tilde{R}, \tilde{Z})$, the flow problem is unsteady. To convert the unsteady state in the fixed frame into the steady state in the wave frame $(\tilde{r}, \tilde{z})$, moving with the same vave speed c, the following linear transformations are introduced as (Akbar and Nadeem 2012; Butt et al. 2020):

$$\begin{aligned}&\tilde{r} = \tilde{R},\ \tilde{z} = \tilde{Z} - c\tilde{t},\ \tilde{u} = \tilde{U},\ \tilde{w} = \tilde{W} - c,\ \tilde{h}(\tilde{z}, \tilde{t})\\ &= \tilde{H}(\tilde{Z}, \tilde{t}),\ \tilde{p}(\tilde{z}, \tilde{r}, \tilde{t}) = \tilde{P}(\tilde{Z}, \tilde{R}, \tilde{t}),\\ &\tilde{T}(\tilde{z}, \tilde{r}, \tilde{t}) = \tilde{T}(\tilde{Z}, \tilde{R}, \tilde{t}),\end{aligned} \tag{15}$$

We introduce non-dimensional variable:

$$\begin{aligned}&r = \frac{\tilde{r}}{\tilde{a}},\ z = \frac{\tilde{z}}{\lambda},\ w = \frac{\tilde{w}}{c},\ u = \frac{\lambda\tilde{u}}{\tilde{a}c},\ p = \frac{\tilde{a}^2\tilde{p}}{c\lambda\mu_f},\ \theta = \frac{\tilde{T}-\tilde{T}_0}{\tilde{T}_0},\ t = \frac{c\tilde{t}}{\lambda},\ \beta = \frac{\tilde{a}}{\lambda},\\ &Re = \frac{c\tilde{a}\rho_f}{\mu_f},\ Br = \frac{c^2\mu_f}{(c_p)_f\tilde{T}_0},\ \tau_{ij} = \frac{\tilde{a}\tilde{\tau}_{ij}}{c\mu_f},\ We = \frac{\Lambda c}{\tilde{a}},\ h = \frac{\tilde{h}}{\tilde{a}},\ \gamma = \frac{Q_0\tilde{a}^2}{k_f\tilde{T}_0},\end{aligned} \tag{16}$$

where *Re* is the Reynolds number which signifies the ratio of the inertial force to the viscous force, *Br* is the Brinkman number that is related to the heat transfer phenomena of the flow field, *We* is the Weissenberg number representing the

ratio of relaxation time to the radius of the tube, and γ is the internal heat source parameter.

In pursuance of Eqs. (1–3) and Eqs. (15–16), Eqs. (10–13) related to the blood flow model under the assumption of long wavelength can be put in the non-dimensional form as (Akbar and Nadeem 2012; Butt et al. 2020):

$$\frac{\partial p}{\partial r} = 0, \tag{17}$$

$$\frac{\partial p}{\partial z} = \frac{1}{r}\frac{\partial}{\partial r}(r\tau_{rz}), \tag{18}$$

$$\frac{x_4}{r}\frac{\partial}{\partial r}\left(r\frac{\partial \theta}{\partial r}\right) + x_2 Br\frac{\partial w}{\partial r}\tau_{rz} + \gamma = 0, \tag{19}$$

$$f\tau_{zz} = 2\,We\tau_{rz}\frac{\partial w}{\partial r}, \tag{20}$$

$$f\tau_{rz} = \frac{\partial w}{\partial r} + We\tau_{rr}\frac{\partial u}{\partial r}, \tag{21}$$

$$f = 1 + \varepsilon We(\tau_{rr} + \tau_{\theta\theta} + \tau_{zz}), \tag{22}$$

The dimensionless form of the physical boundary conditions become (Hanasoge et al. 2017):

$$\frac{\partial w}{\partial r} = 0,\ \frac{\partial \theta}{\partial r} = 0,\ \text{at } r = 0,$$
$$w = -1 - \frac{2\pi\delta\alpha\beta\cos(2\pi z)}{1 - 2\pi\delta\alpha\beta\cos(2\pi z)},\ \theta = 0 \text{ at } r = h(z) = 1 + \delta\cos(2\pi z), \tag{23}$$

where β is the wave number.

The integration of the longitudinal momentum Eq.(18) subject to the boundary conditions $\tau_{rz} = 0$ at the symmetry line $r = 0$ yields:

$$\tau_{rz} = \frac{r}{2}\frac{dp}{dz}, \tag{24}$$

By neglecting the wave number β, we get $\tau_{\theta\theta} = 0$, and $\tau_{rr} = 0$, and thus trace of stress tensor becomes τ_{rz}. Eqs. (20) and (21) together imply:

$$\tau_{zz} = 2\,We\,\tau_{rz}^2, \tag{25}$$

Inserting Eqs. (22) and (25) in Eq. (21), one has

$$\frac{\partial w}{\partial r} = \tau_{rz} + 2\varepsilon We^2\tau_{rz}^3, \tag{26}$$

Substituting Eq. (24) into Eq. (26), the velocity gradient takes the form:

$$\frac{\partial w}{\partial r} = \frac{r}{2}\frac{dp}{dz} + 2\varepsilon We^2\left(\frac{r}{2}\frac{dp}{dz}\right)^3, \tag{27}$$

The type I and type II models for the thermo-physical properties suitable for studying the dynamics of hybrid nano-blood are given in Table 1.

where ϕ_1 and ϕ_2 designate the solid volume fractions of copper and silver nanoparticles, respectively. The suffices s_1, s_2, f, nf, hnf denote solid nanoparticles of copper (Cu), solid nanoparticles of silver (Ag), base fluid (blood), nano-blood, and hybrid nano-blood, respectively. The case $\phi_1 = \phi_2 = 0$ (without suspension of nanoparticles) corresponds to the pure-blood. Moreover, in the present study, it is assumed that the nanoparticles are in thermal equilibrium and no-slip occurs between them. The thermo-physical properties are given in Table 2.

Table 2 Thermo-physical properties of blood, copper nanoparticles (Cu), and silver nanoparticles (Ag)Saleem et al. (2020)

properties	Blood	Cu	Ag
$\rho(kg/m^3)$	1063	8933	10500
$c_p(J/kgK)$	3594	385	235
$k(W/mK)$	0.492	401	429

Table 1 Models of nano-blood (Type I) and hybrid nano-blood (Type II) (Xu and Sun 2019; Shah et al. 2020)

Thermo-physical properties	Type I correlation (Cu-blood nanofluid)	Type II correlation (Cu-Ag/blood hybrid nanofluid)
Density	$\rho_{nf} = (1-\phi_1)\rho_f + \phi_1\rho_{s_1}$	$\rho_{hnf} = (1-\phi_2)[(1-\phi_1)\rho_f + \phi_1\rho_{s_1}] + \phi_2\rho_{s_2}$
Viscosity	$\mu_{nf} = \frac{\mu_f}{(1-\phi_1)^{2.5}}$	$\mu_{hnf} = \frac{\mu_f}{(1-\phi_1)^{2.5}(1-\phi_2)^{2.5}}$
Heat capacity	$(\rho c_p)_{nf} = (1-\phi_1)(\rho c_p)_f + \phi_1(\rho c_p)_{s_1}$	$(\rho c_p)_{hnf} = (1-\phi_2)[(1-\phi_1)(\rho c_p)_f + \phi_1(\rho c_p)_{s_1}] + \phi_2(\rho c_p)_{s_2}$
Thermal conductivity	$k_{nf} = k_f\left[\frac{k_{s_1}+2k_f-2\phi_1(k_f-k_{s_1})}{k_{s_1}+2k_f+\phi_1(k_f-k_{s_1})}\right]$	$k_{hnf} = k_{bf}\left[\frac{k_{s_2}+2k_{bf}-2\phi_2(k_{bf}-k_{s_2})}{k_{s_2}+2k_{bf}+\phi_2(k_{bf}-k_{s_2})}\right]$ where $k_{bf} = k_f\left[\frac{k_{s_1}+2k_f-2\phi_1(k_f-k_{s_1})}{k_{s_1}+2k_f+\phi_1(k_f-k_{s_1})}\right]$

3 Exact solution

On integrating Eq.(27) and employing the boundary conditions (23), the exact solution for the velocity field is obtained as follows:

$$w(r,z) = \frac{1}{16}We^2\varepsilon\left(\frac{dp}{dz}\right)^3\left(r^4-h^4\right)+\frac{1}{4}\left(\frac{dp}{dz}\right)\left(r^2-h^2\right)-1-\frac{2\pi\delta\alpha\beta\cos(2\pi z)}{1-2\pi\delta\alpha\beta\cos(2\pi z)}, \tag{28}$$

After using Eq.(28) in Eq.(19), and solving, we achieve the temperature distribution of the blood flow as:

$$\theta(r,z) = \frac{1}{576\,x_4}\left[2\,\varepsilon\,x_2\,Br\,We^2\left(\frac{dp}{dz}\right)^4\left(h^6-r^6\right)+9\,x_2\,Br\left(\frac{dp}{dz}\right)^2\left(h^4-r^4\right) + 144\,\gamma\left(h^2-r^2\right)\right], \tag{29}$$

3.1 Flow rate, stream function, and heat transfer

The volume flow rate Q can be calculated as

$$Q = 2\int_0^h r\,w(z,r)dr, \tag{30}$$

which gives the expression for the pressure gradient as

$$\frac{dp}{dz} = \frac{A}{h^6We^2\varepsilon}-\frac{h^4}{A}, \tag{31}$$

where

$$A = \left(12h^{12}We^4\varepsilon^2B+\sqrt{h^{24}We^6\varepsilon^3\left(h^6+144We^2\varepsilon B^2\right)}\right)^{1/3},\ B = \left(h^2X-Q\right),$$
$$X = -\frac{2\pi\alpha\beta\delta\cos(2\pi z)}{1-2\pi\alpha\beta\delta\cos(2\pi z)}-1, \tag{32}$$

The mean volume flow rate over one period of the peristaltic wave is defined as

$$F = Q+\frac{1}{2}\left(\frac{\delta^2}{2}+1\right), \tag{33}$$

The dimensionless pressure rise Δp over one period of wavelength can be expressed as

$$\Delta p = \int_0^1 \frac{dp}{dz}\,dz, \tag{34}$$

Due to the complication of the expression (34), the symbolic software Mathematica has been deployed to assess the numerical integration of the pressure-rise.

The velocity components are expressed in terms of the stream-function and are mathematically defined as

$$u = -\frac{1}{r}\frac{\partial\psi}{\partial r},\ w = \frac{1}{r}\frac{\partial\psi}{\partial r}, \tag{35}$$

To obtain the stream function ψ, we integrate $w = \frac{1}{r}\frac{\partial\psi}{\partial r}$ with $\psi = 0$ at $r = 0$, and then the stream function is given by

$$\psi = \frac{1}{48}r^2\left[We^2\varepsilon\left(\frac{dp}{dz}\right)^3\left(r^4-3h^4\right)+6\frac{dp}{dz}\left(r^2-2h^2\right)+48X\right], \tag{36}$$

The stream function represents the volumetric flow rate through the cross section bounded by the ciliated tube wall.

The heat transfer coefficient at the wall of ciliated tube is computed as:

$$Z^* = \frac{k_{hnf}}{k_f}\frac{dh}{dz}\left(\frac{\partial\theta}{\partial r}\right)_{r=h} = \frac{1}{24}\pi\delta h\sin(2\pi z)\left[Br\left(\frac{dp}{dz}\right)^2h^2x_2\left\{\left(\frac{dp}{dz}\right)^2h^2We^2\varepsilon+3\right\}+24\gamma\right], \tag{37}$$

3.2 Entropy generation

Non-equilibrium situation emerges as a result of the exchange of momentum, and temperature within the hybrid nano-blood and at the wall of the ciliated tube which causes a continuous entropy generation (EG). The volumetric entropy generation (EG) term (E_G) can be calculated as follows:

$$E_G = \underbrace{\frac{k_{hnf}}{\tilde{\theta}_0^2}\left\{\left(\frac{\partial\tilde{T}}{\partial\tilde{r}}\right)^2+\left(\frac{\partial\tilde{T}}{\partial\tilde{z}}\right)^2\right\}}_{\text{Thermal irreversibility}}+\underbrace{\frac{1}{\tilde{\theta}_0}\tilde{\tau}_{\tilde{r}\tilde{z}}\frac{\partial\tilde{w}}{\partial\tilde{r}}}_{\text{Fluid friction irreversibility}}, \tag{38}$$

Utilizing non-dimensional variables in Eq.(16), the entropy generation number can be expressed as

$$E_G = E_g\left[x_4\left(\frac{\partial\theta}{\partial r}\right)^2+x_2Br\zeta\tau_{rz}\frac{\partial w}{\partial r}\right], \tag{39}$$

where $E_g = \frac{k_f \bar{T}_0^2}{\tilde{\theta}_0^2 \tilde{a}^2}$, and $\zeta = \frac{\tilde{\theta}_0}{\bar{T}_0}$ are the characteristic entropy generation rate and the dimensionless temperature difference, respectively.

Entropy gives the degree of disorder of the system and its surroundings. The rate of dimensionless entropy formation is as follows

$$N_S = \frac{E_G}{E_g}, = \frac{r^2}{2304 x_4}\left[Br\left(\frac{dp}{dz}\right)^4 r^4 We^2 x_2 \varepsilon + 3Br\left(\frac{dp}{dz}\right)^2 r^2 x_2 + 24\gamma\right]^2 + \frac{1}{8}Br\left(\frac{dp}{dz}\right)^2 \zeta r^2 x_2 \left[\left(\frac{dp}{dz}\right)^2 r^2 We^2 \varepsilon + 2\right], \tag{40}$$

One more significant pertinent parameter is Bejan number *Be*, which is the ratio of heat and mass transfer and it is given by

$$Be = \frac{r^2}{2304 x_4}\left[Br\left(\frac{dp}{dz}\right)^4 r^4 We^2 x_2 \varepsilon + 3Br\left(\frac{dp}{dz}\right)^2 r^2 x_2 + 24\gamma\right]^2 / \left\{\frac{r^2}{2304 x_4}\left[Br\left(\frac{dp}{dz}\right)^4 r^4 We^2 x_2 \varepsilon + 3Br\left(\frac{dp}{dz}\right)^2 r^2 x_2 + 24\gamma\right]^2 + \frac{1}{8}Br\left(\frac{dp}{dz}\right)^2 \zeta r^2 x_2 \left[\left(\frac{dp}{dz}\right)^2 r^2 We^2 \varepsilon + 2\right]\right\}, \tag{41}$$

4 Validation of results

In order to verify the validity of this research study, we have considered some particular cases. The results of Butt et al. (2020) are recovered by deputizing $\gamma = \phi_1 = \phi_2 = 0$. Our results are in an excellent covenant with the Ref. Butt et al. (2020). Furthermore, we have attempted to check the correctness of the present results by comparing them to those previously recorded by Akbar and Butt (2014). The results of the present model and those of Akbar and Butt (2014) show a good deal of agreement via Fig. 2a–b. This graphical comparison asserts the authenticity about the perfection of the present study.

5 Analysis and Discussion of Results

This segment is devoted to explore the significant flow characteristics, viz. the axial velocity profile, temperature profile, pressure gradient, pressure rise, heat transfer coefficient, entropy generation, Bejan number, and streamline structure under variation of emerging thermo-physical parameters/constraints through the graphical expositions and physical interpretations. For graphical computation, the default estimations of non-dimensional quantities/parameters are selected based on Butt et al. (2020): $\phi_1 = 0.02$, $\phi_2 = 0.02$, $\varepsilon = 0.1, \alpha = 0.1, \beta = 0.2, \delta = 0.1, F = 0.5, We = 1, Br = 0.2$, $z = 0.75, \gamma = 0.5$ and $\zeta = 0.2$. In addition, $\phi_1 = \phi_2 = 0$ corresponds to pure blood, $\phi_1 = 0.01$, $\phi_2 = 0$ for Cu-blood, and $\phi_1 = 0.01$, $\phi_2 = 0.02$ for Cu-Ag/blood. The graphical presentations are performed through computational software *Mathematica*.

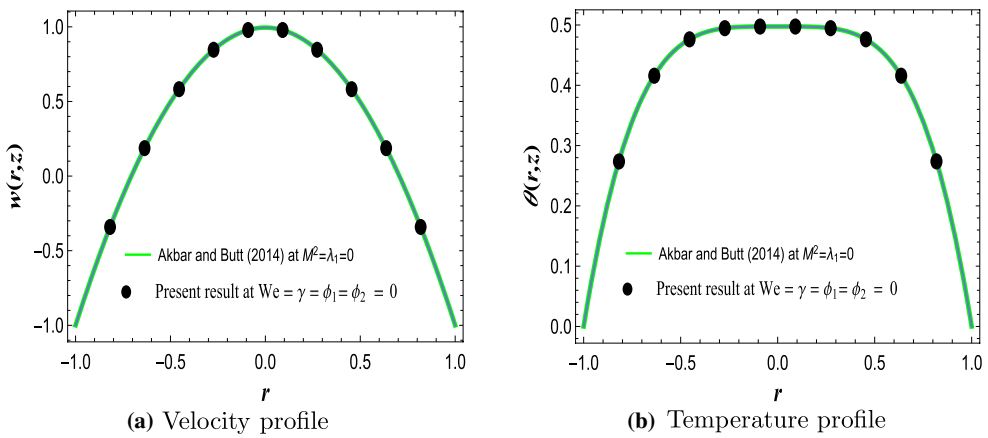

(a) Velocity profile **(b)** Temperature profile

Fig. 2 Comparison of velocity and temperature profiles with $\phi_1 = 0.0$, $\phi_2 = 0.0$, $We = 0$, $\varepsilon = 0.1$, $\alpha = 0.1$, $\beta = 0.2$, $\delta = 0.1$, $F = 0.5$, $Br = 0.2$, $z = 0.75$, $\gamma = 0.5$

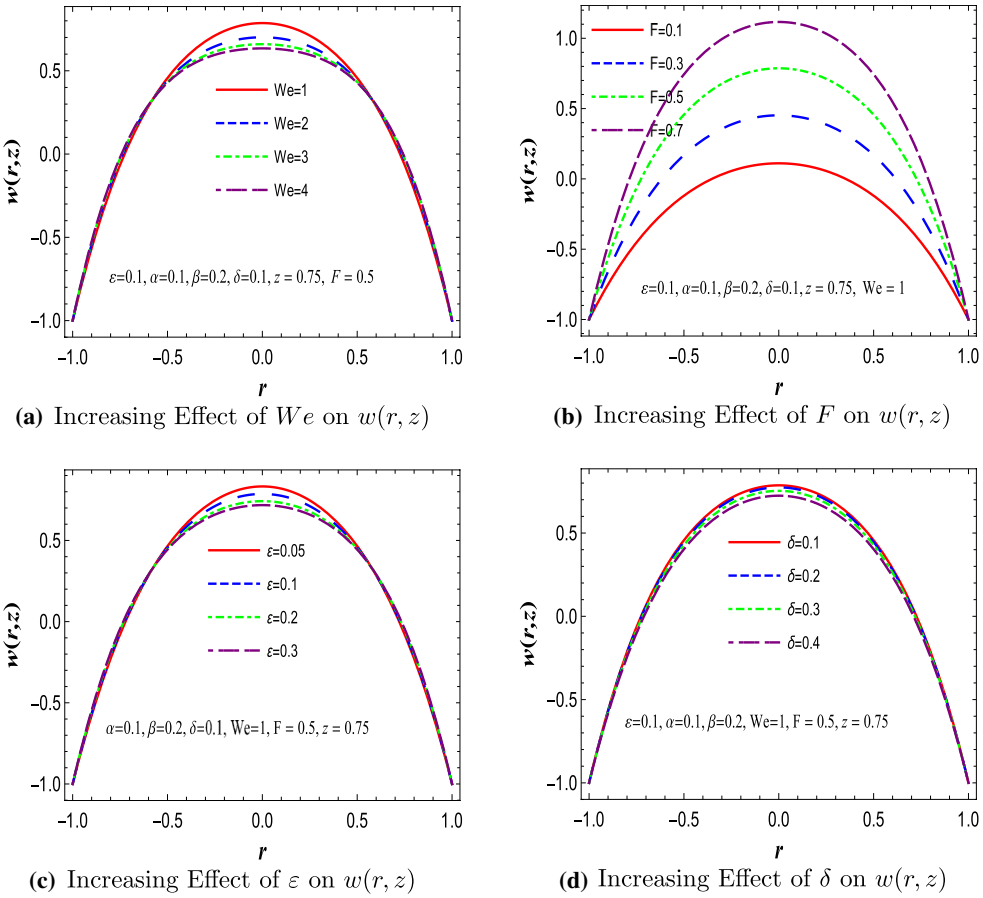

(a) Increasing Effect of We on $w(r, z)$ **(b)** Increasing Effect of F on $w(r, z)$

(c) Increasing Effect of ε on $w(r, z)$ **(d)** Increasing Effect of δ on $w(r, z)$

Fig. 3 Variation of axial velocity profile $w(r, z)$ for different physical parameters

5.1 Axial velocity profile

Figure 3a–d are exposed to analyze the effects of different increasing emerging dynamical parameters, viz. Weissenberg number *We*, mean flow rate F, Phan-Thien-Tanner (PTT) elongation parameter ε, and cilia length δ on the non-dimensional velocity field $w(r, z)$. The dependency of velocity field on Weissenberg number *We* is demonstrated in Fig. 3a. The curves in this figure manifest that the velocity field diminishes for upsurging *We* and gets its maximum value at the center of the tube. The Weissenberg number is a proportion of relaxation time to the radius of the tube. Growing *We* increases the relaxation time of the blood particles, which enhances viscosity and generates resistance to the blood flow, resulting in a decrement in blood velocity. Furthermore, a reversal of the outcome is detected near the ciliated tube wall because the radius of the ciliated tube is inversely related to *We*. To disclose the variation of the velocity field for viscous dumping parameter *F*, Fig. 3b is designed. An increment in *F* exhibits an uplifting trend in the velocity field within the flow domain. For greater *F*, less resistive force is perceived within the ciliated tube and consequently, the velocity profile enhances. The consequence of PTT elongation parameter ε on velocity field is sketched in Fig. 3c. Increasing ε augments the velocity profile near the ciliated tube wall but lessens these curves at the central domain. These features are similar to the outcome of *We*, which is quite expected as ε is proportional to *We* in Phan-Thien-Tanner (PTT) model. Fig. 3d divulges the variation of the velocity field for increasing cilia length parameter δ. Boosted δ shows the declining feature on the velocity field throughout the flow domain. The larger δ produces more resistance in the flow region which causes a diminution in the velocity field.

5.2 Temperature profile

In this subsegment, Fig. 4a–g are sketched to demystify the effects of various emerging physical parameters like Weissenberg number *We*, Brinkman number *Br*, mean flow rate F, heat source parameter γ, Phan-Thien-Tanner (PTT) elongation parameter ε, cilia length δ, and nanoparticle volume fractions (ϕ_1, ϕ_2) on the non-dimensional temperature field $\theta(r, z)$. The temperature field is the measure of the average

Fig. 4 Variation of temperature profile $\theta(r, z)$ for different physical parameters

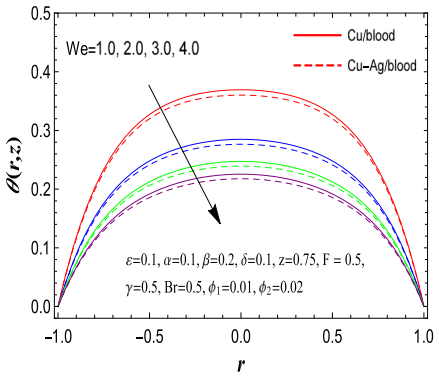

(a) Increasing Effect of We on $\theta(r, z)$

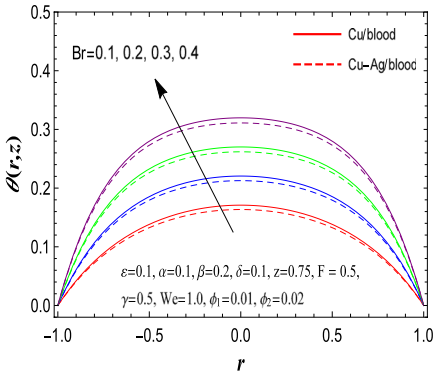

(b) Increasing Effect of Br on $\theta(r, z)$

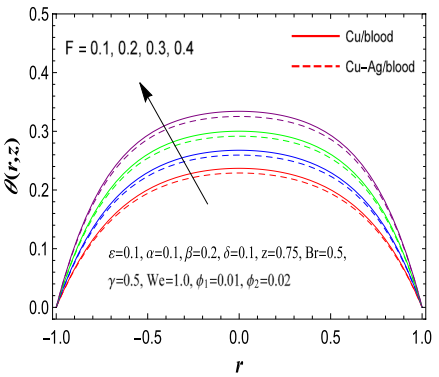

(c) Increasing Effect of F on $\theta(r, z)$

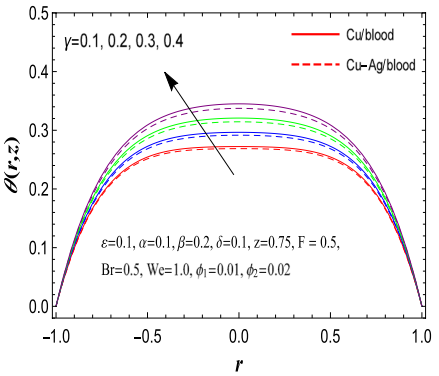

(d) Increasing Effect of γ on $\theta(r, z)$

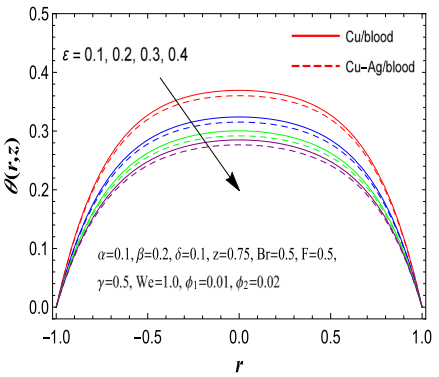

(e) Increasing Effect of ε on $\theta(r, z)$

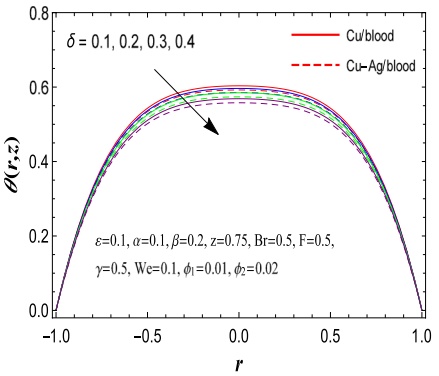

(f) Increasing Effect of δ on $\theta(r, z)$

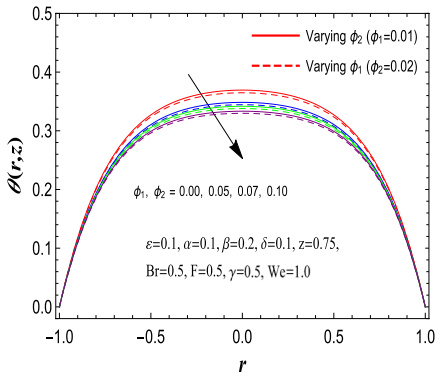

(g) Increasing Effect of ϕ_1 and ϕ_2 on $\theta(r, z)$

kinetic energy of the blood cells, copper and silver nanoparticles present in the hybrid nano-blood (Cu-Ag/blood). Fig. 4a discloses the impact of increasing Weissenberg number *We* on the temperature field. It is detected from the pictorial representation that the temperature field is greatest at the central region of the ciliated tube and least nearby the ciliated walls. For larger *We*, the relaxation time of the hybrid nano-blood particles increases which generates resistance to flow particles and reduces the kinetic energy, as a result, the temperature field significantly declines. Influence of elevating Brinkman number *Br* on the temperature field is reflected in Fig. 4b. Incremented *Br* boosted up the temperature profile. Brinkman number is the proportion of viscous heat generation to heat transport due to molecular conduction. Hence greater estimation of *Br* slows down the heat conduction (i.e., the diffusion of thermal(heat) energy) which is suppressed by viscous dissipation and consequently, the average kinetic energy of hybrid nano-blood particles enhances and temperature profile gets an increment. Figure 4c demonstrates the variation of temperature field for increasing viscous dumping parameter *F*. An increment in *F* accomplishes an augmentation in the temperature field. The impact of the heat source parameter γ on the temperature profile is reflected in Fig. 4d. This pictorial presentation clarifies that increasing γ shows an ascending trend in the temperature profile. The temperature field earns its maximum value at the central line of the ciliated tube and gradually decreases toward the wall. It happens due to more heat generation within hybrid nano-blood which warms up the molecules or particles and enhances the average kinetic energy of the molecules or particles, when the internal heat source increases. The dependency of the PTT elongation parameter ε on temperature field is graphed in Fig. 4e. Thriving ε tends to a diminution in blood temperature. Fig. 4f demonstrates the upshot of increasing cilia length δ on the temperature field. Larger estimations of cilia length δ induce a remarkable declination in the blood temperature at the central region of the ciliated tube because an increment in cilia length generates resistance to the hybrid nano-blood particles movement which reduces average kinetic energy. The effectiveness of nanoparticle volume fractions ϕ_1 and ϕ_2 on the temperature profile is depicted in Fig. 4g. The blood temperature field declines considerably for evolving ϕ_1 or ϕ_2. For larger ϕ_1 or ϕ_2, the thermal conductivity improves and the nano-blood becomes more viscous which induces resistance to the flow field. Consequently, the average kinetic

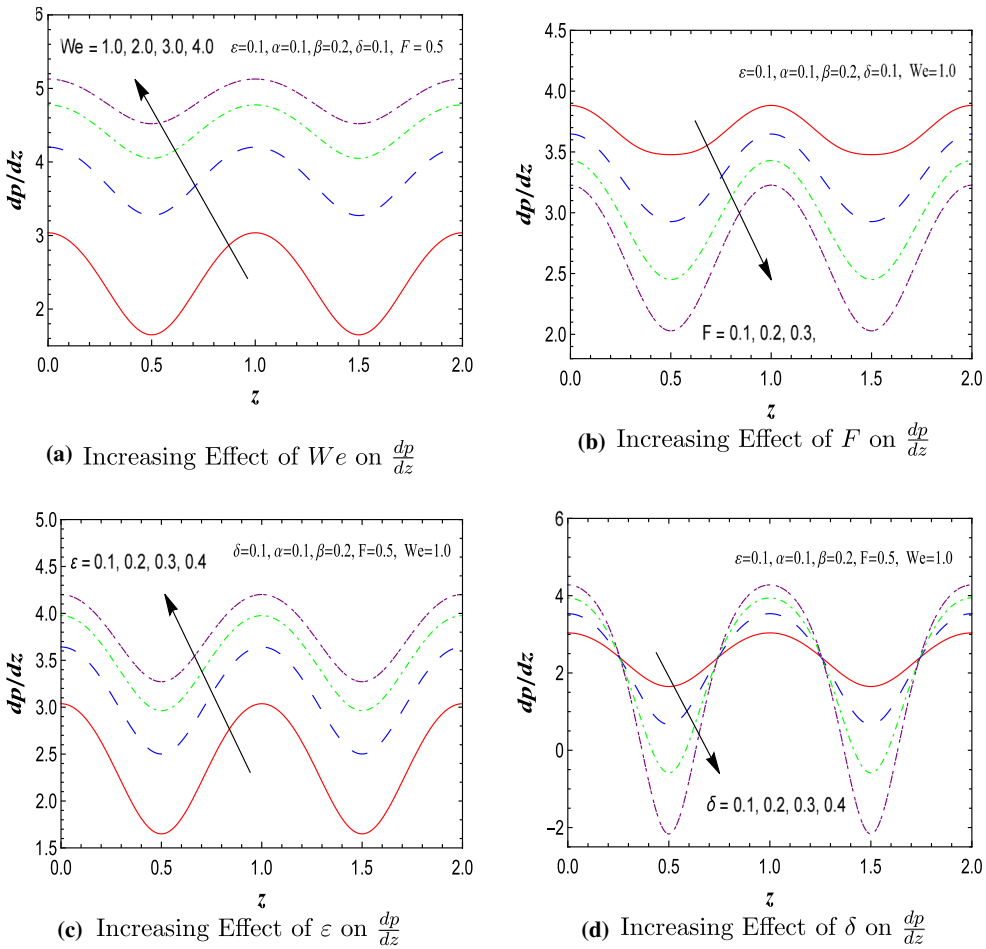

(a) Increasing Effect of We on $\frac{dp}{dz}$

(b) Increasing Effect of F on $\frac{dp}{dz}$

(c) Increasing Effect of ε on $\frac{dp}{dz}$

(d) Increasing Effect of δ on $\frac{dp}{dz}$

Fig. 5 Variation of pressure gradient $\frac{dp}{dz}$ for different physical parameters

energy decreases, and temperature field gets an intensive decrement. From Fig. 4a–f, it can be perceived that the hybrid nano-blood (Cu- Ag/blood) accomplishes lower temperature compared to nano-blood (Cu-blood) because hybrid nano-blood possess more viscous nature than nano-blood. These results also demonstrate that the concentration of hybrid nanoparticles in the blood is preferable to the concentration of mono nanoparticles due to a significant improvement in the thermal properties of the blood flow. The physical reason for this activity is that as blood flows away from the ciliated tube wall, nanoparticles near the ciliated tube wall heat up, increasing blood flow away from the ciliated tube wall and decreasing the temperature gradient. Furthermore, Ag nanoparticles have a higher atomic number, which induces a significant decline in the temperature profile of blood. As a result, when compared to Cu nanoparticles, Ag nanoparticles have better thermal properties. Such a finding is extremely beneficial to the cancer care process (Ag nanoparticles as a drug carrier).

5.3 Pumping characteristics

5.3.1 Axial pressure gradient

Figure 5a–d presents the variation of the pressure gradient $\frac{dp}{dz}$ along the length of the ciliated tube under the impact of Weissenberg number *We*, mean flow rate *F*, Phan-Thien-Tanner (PTT) elongation parameter ε, and cilia length δ. Figure 5a illustrates the physical consequence of Weissenberg number *We* on the pressure gradient. An augmented *We* tends to boost the pressure gradient. On the contrary, Fig. 5b explores the descending behavior of boosted mean flow rate *F* on the pressure gradient. The impression of the augmented PTT elongation parameter ε on the pressure gradient is disclosed in Fig. 5c. It is witnessed from the pictorial illustration that the pressure gradient is directly related to the PTT elongation parameter. Meanwhile, the pressure gradient at the central line of the ciliated tube, as visualized in Fig. 5d, enhances and then starts to oscillate gradually to the wall with incrementing cilia length δ.

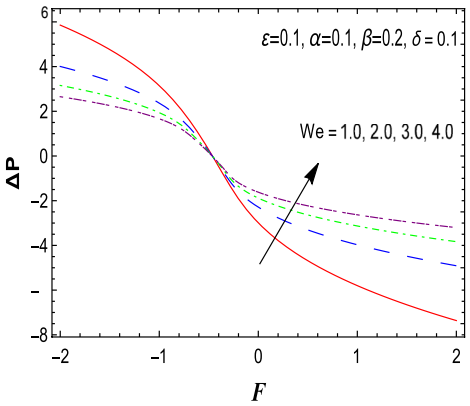

(a) Increasing Effect of We on ΔP

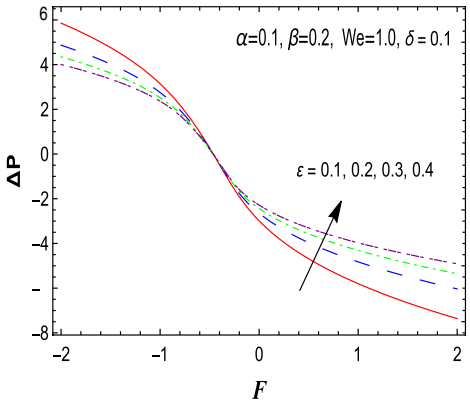

(b) Increasing Effect of ε on ΔP

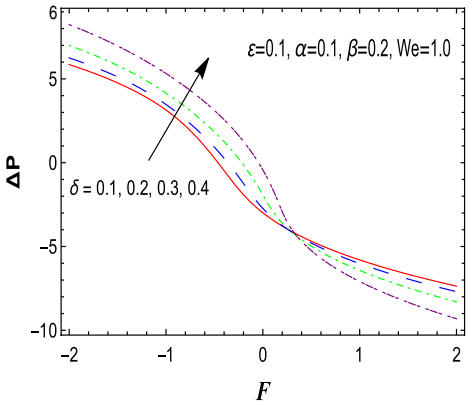

(c) Increasing Effect of δ on ΔP

Fig. 6 Variation of pressure rise ΔP for different physical parameters

Fig. 7 Variation of heat transfer coefficient Z^* for different physical parameters

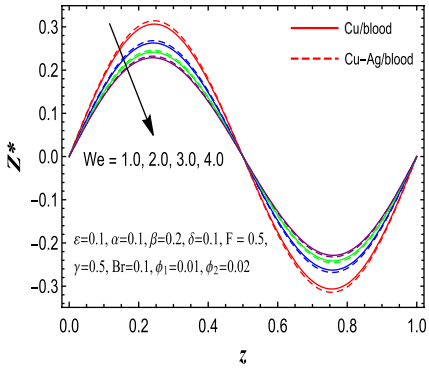

(a) Increasing Effect of We on Z^*

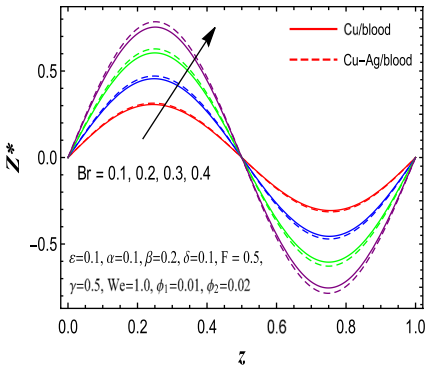

(b) Increasing Effect of Br on Z^*

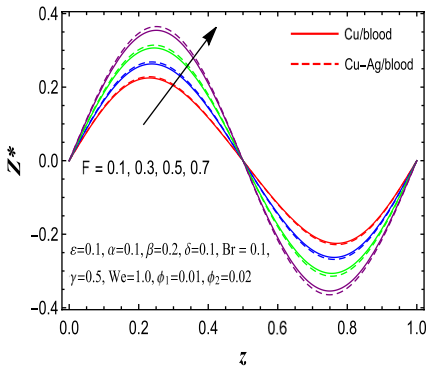

(c) Increasing Effect of F on Z^*

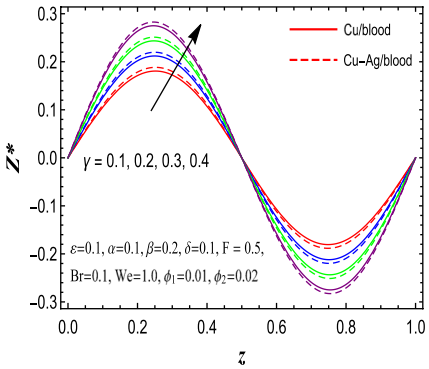

(d) Increasing Effect of γ on Z^*

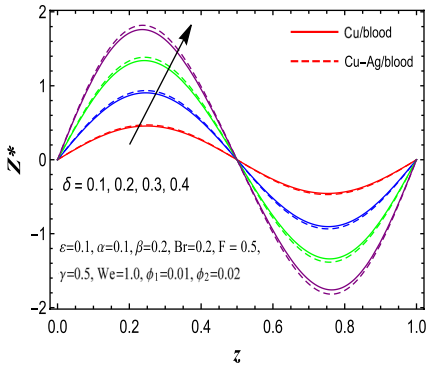

(e) ncreasing Effect of δ on Z^*

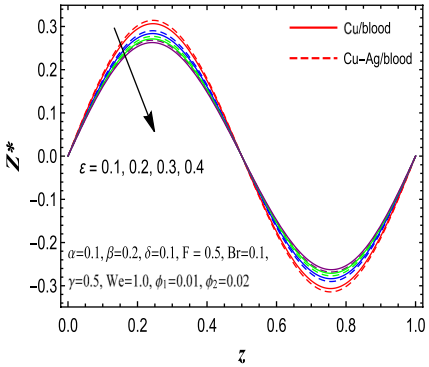

(f) Increasing Effect of ε on Z^*

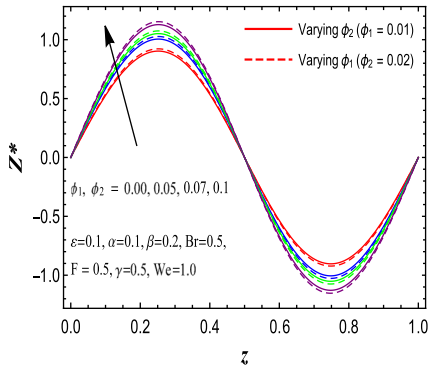

(g) Increasing Effect of ϕ_1 and ϕ_2 on Z^*

5.3.2 Pressure rise per wavelength

The pressure rise ΔP (i.e., pressure difference across single wavelength) is a significant physical measure in the peristaltic pumping mechanism. The variation in the pressure rise ΔP with mean flow rate F under the respective influence of Weissenberg number We, Phan-Thien-Tanner (PTT) elongation parameter ϵ, and cilia length δ is depicted in Fig. 6a–c. Figure 6a demystifies a decrement in pressure rise by energized Weissenberg number We in the region $-2 \leq F \leq -0.45$ while reversed behavior is detected when $-0.45 \leq F \leq 2$. It can be witnessed from Fig. 6b that the pressure rise lessens with an increase in PTT elongation parameter ϵ in the region ($\Delta P > 0,\ F < -0.45$). However, a contrary trend is disclosed in the region ($\Delta P < 0,\ F > -0.45$). Figure 6c clarifies that higher estimations of cilia length δ tend to boost the pressure rise in the pumping zone $-2 \leq F \leq -0.32$ but expose a declination in the region $-0.32 \leq F \leq 2$.

5.4 Heat transfer coefficient

The variations of the heat transfer coefficient Z^* at the wall of the ciliated tube for various values of We, Br, F, γ, δ, ϵ, ϕ_1, and ϕ_2 against z are publicized via Fig. 7a–g. The absolute value of the heat transfer coefficient $|Z^*|$ declines with an increment in We, and ϵ, but a contrary behavior is witnessed for greater values of Br, F, γ, δ, ϕ_1 and ϕ_2. A mounted Br boots the kinetic energy of nanoparticles which expedites $|Z^*|$. The minimum of $|Z^*|$ associates to a lower volume fraction of both nanoparticles in the blood. It is also notable that the feature of heat transport is oscillatory. This behavior is under the physical expectation due to metachronal waves traveling along the ciliated tube (stimulated by the power and recovery strokes of evenly distributed cilia lined in the tube wall). The heat transfer coefficient $|Z^*|$ for hybrid nano-blood (Cu-Ag/blood) is higher compared to nano-blood (Cu-blood).

5.5 Entropy generation and Bejan Number

In this subsegment, the variations of entropy generation Ns and Bejan number Be for mounted values of We, F, Br, γ, ζ, δ, ϕ_1, and ϕ_2 are illustrated via Fig. 8a–n. Figure 8a indicates the descending behavior of total entropy number near the ciliated tube wall but no effect at the center for increasing Weissenberg number We. It is also remarkable that maximum value of Ns is detected at the wall of the tube. Fig. 8b shows a decrement in the proximity of the tube wall but an opposite behavior at the center for Bejan number Be when We increases. An augmentation in the mean flow rate F tends to boost both Ns and Be near the tube wall as plotted in Fig. 8c–d. Further, at the center of the tube ($r = 0$), the entropy number does not respond and the Bejan number reduces significantly for growing F. The variations of Brinkman number Br on total entropy number and Bejan number are reflected in Fig. 8e–f Increasing Br markedly upsurges the total entropy number and Bejan number near the ciliated tube wall. A diminution in Be at the center of the ciliated tube is observed due to enhancement in Br. The dependency of heat source γ on total entropy number and Bejan number is disclosed via Fig. 8g–h. Both the quantities Ns and Be are upsurged for increasing heat source γ. For higher temperature difference parameter ζ, as publicized in Fig. 8i–j, total entropy number Ns enhances except the center of the tube but Bejan number Be declines throughout the flow domain. Fig. 8k–l is designed to demonstrate the variation of the total entropy number and Bejan number for thriving cilia length δ. It is noted from these curves that Ns decelerates with incrementing cilia length δ. Moreover, as disclosed in Fig. 8l, Bejan number Be is found to upsurge owing to augmenting δ except the proximity of the ciliated tube wall. The effectiveness of volume fractions of suspended nanoparticles ϕ_1 and ϕ_2 on the total entropy number and Bejan number is graphed in Fig. 8m–n. By an increment in ϕ_1 and ϕ_2, total entropy number Ns expedites within the ciliated tube except for the center ($r = 0$) but a contrary trend is detected for Bejan number Be. It is worth mentioning that the entropy generation number tends to zero at the center-line of the tube and gradually increases as it tends to the tube wall and attains its maximum at the wall. It is also witnessed that hybrid nano-blood exhibits a greater total entropy number than nano-blood. The contrary behavior is marked in the case of the Bejan number.

In Fig. 9a–b, 3D surface plots of total entropy generation number Ns and Bejan number Be are depicted. Figure 9a exposes that supremum estimation of Ns is noted at the narrow segment of the ciliated tube and in the wider segment it reaches its least value. This clarifies that the compressed segment of the tube is found to boost the entropy number. In Fig. 9b, the Bejan number is imprinted against r and z variables. It discloses that at the compressed part of the tube, the impact of heat transfer irreversibility is dominated, but, in the expanded segment of the tube, heat transfer irreversibility declines and the blood friction irreversibility gradually upsurges.

5.6 Streamlines pattern

Trapping is an interesting manifestation of cilia-assisted pumping flow, which does not occur below the critical flow rate. It is the development of a bolus of blood confined by the closed and internally circulating streamlines and driven forward along with the metachronal wave. To disclose the trapping feature, streamlines pattern of the blood flow have been visualized for various values of We, F, β, and δ via Fig. 10a–h. Figure 10a–b are portrayed to

Fig. 8 Variation of entropy generation and Bejan number for different physical parameters

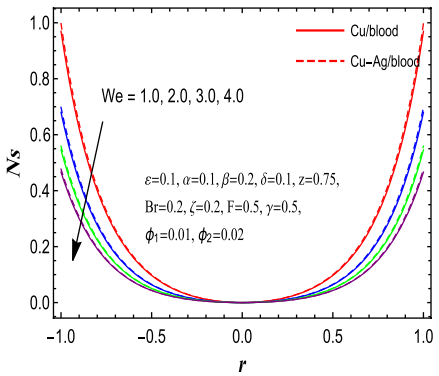

(a) Increasing Effect of We on Ns

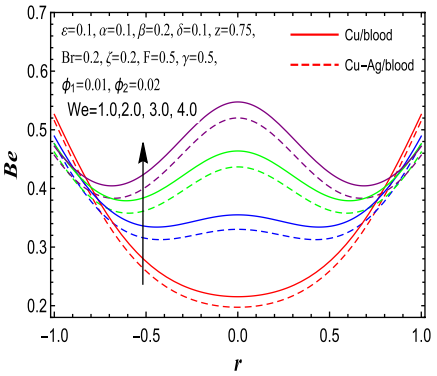

(b) Increasing Effect of We on Be

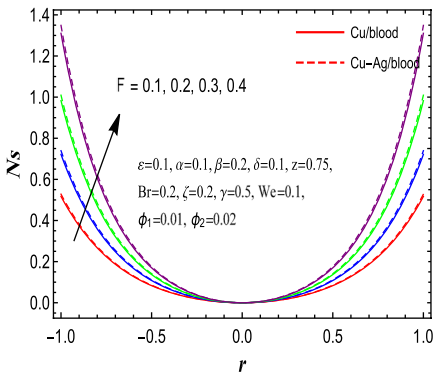

(c) Increasing Effect of F on Ns

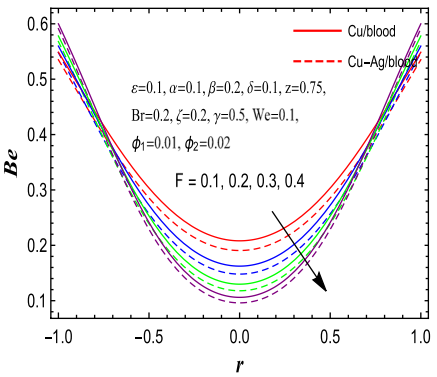

(d) Increasing Effect of F on Be

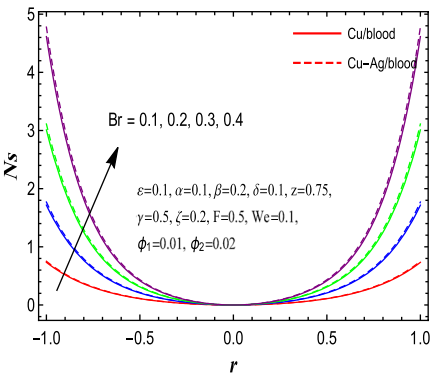

(e) Increasing Effect of Br on Ns

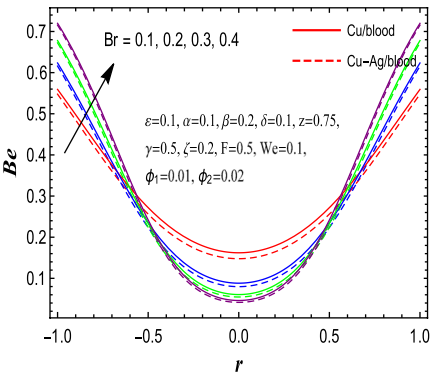

(f) Increasing Effect of Br on Be

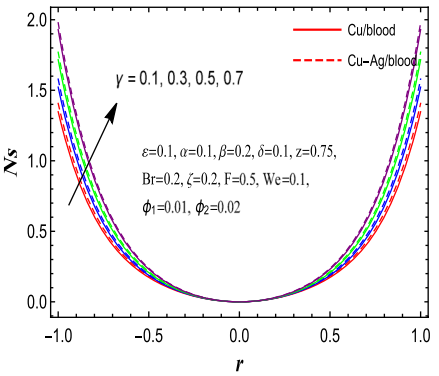

(g) Increasing Effect of γ on Ns

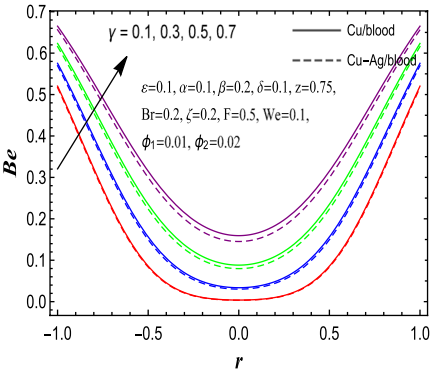

(h) Increasing Effect of γ on Be

Fig. 8 (continued)

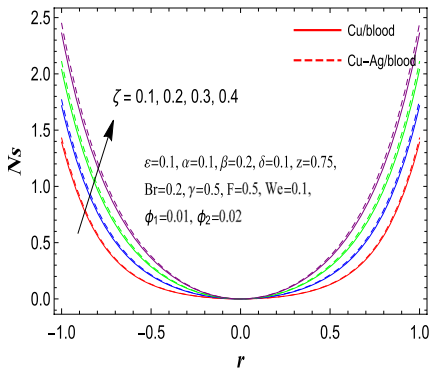

(i) Increasing Effect of ζ on Ns

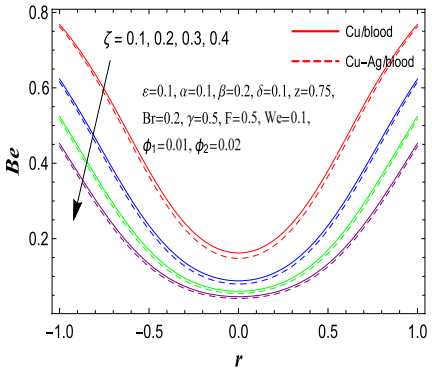

(j) Increasing Effect of ζ on Be

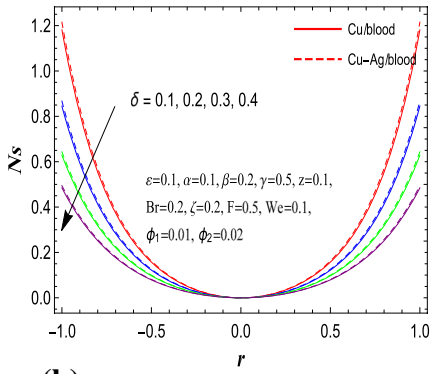

(k) Increasing Effect of δ on Ns

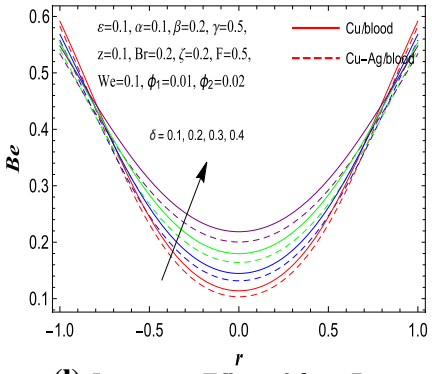

(l) Increasing Effect of δ on Be

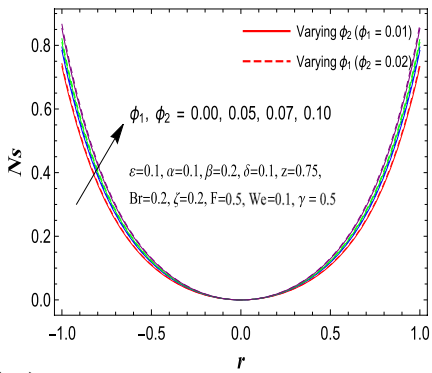

(m) Increasing Effect of ϕ_1 and ϕ_2 on Ns

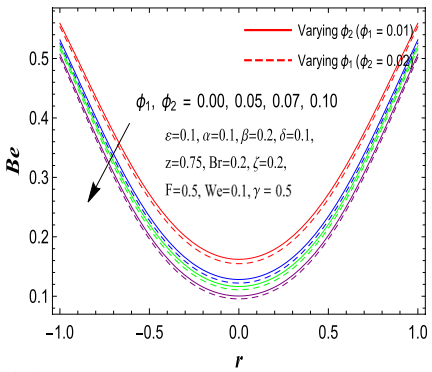

(n) Increasing Effect of ϕ_1 and ϕ_2 on Be

Fig. 9 Surface plot of entropy generation and Bejan number, when $\varepsilon = 0.1$, $\alpha = 0.1$, $\beta = 0.2$, $\delta = 0.1$, $z = 0.75$, $Br = 0.2$, $\zeta = 0.2$, $F = 0.5$, $We = 0.1$, $\gamma = 0.5$, $\phi_1 = 0.01$ and $\phi_2 = 0.02$

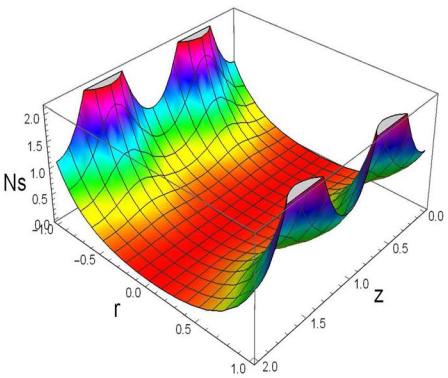

(a) Surface plot for Ns

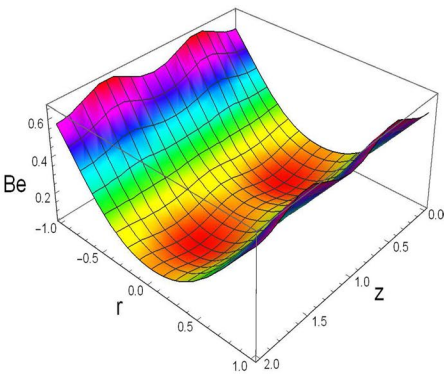

(b) Surface plot for Be

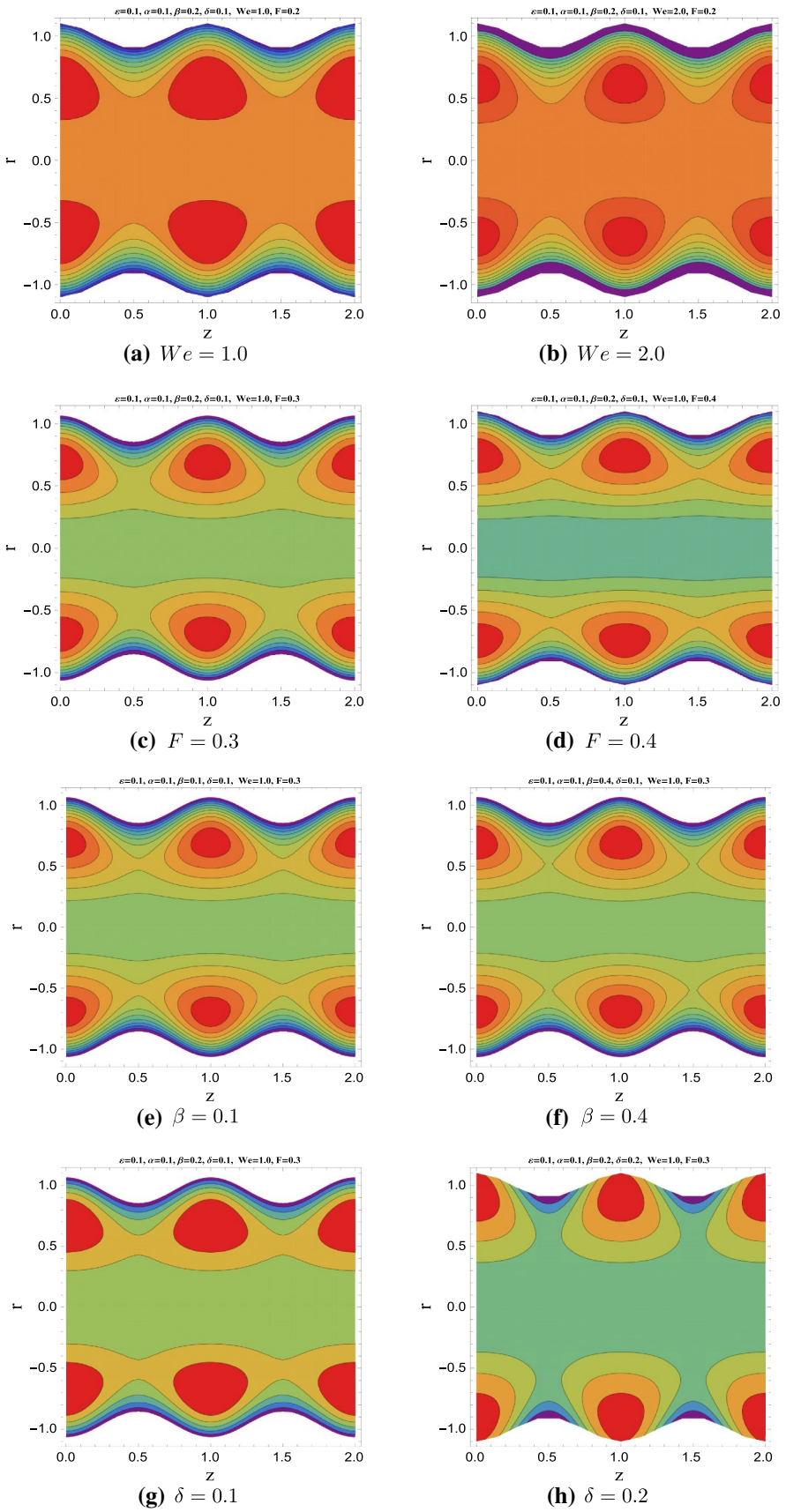

(a) $We = 1.0$ **(b)** $We = 2.0$

(c) $F = 0.3$ **(d)** $F = 0.4$

(e) $\beta = 0.1$ **(f)** $\beta = 0.4$

(g) $\delta = 0.1$ **(h)** $\delta = 0.2$

Fig. 10 Streamlines for different physical parameters

disclose the streamlines pattern for increasing values of Weissenberg number *We*. It is watched that number and size of trapped bolus increase for an elevated *We* which indicates a higher flow rate. Physically, Weissenberg number is proportional to the relaxation time of fluid particles. An increment in Weissenberg number increases the relaxation time of the blood particles and viscoelastic properties of blood become more significant which generates a drag force to the blood particles so that number and size of trapped bolus enhance. The impression of mean flow rate F on streamlines is depicted in Fig. 10c–d. On contrary, the number of imprisoned bolus reduces with an increment in F. Moreover, for a higher mean flow rate, the size of the bolus lessens. The upshot of β on streamlines is exposed in Fig. 10e–f. A mounted β energizes the trapped bolus in size as well as in number. Fig. 10g–h explore that the trapped bolus size and number are significantly increased when the cilia length δ enlarges. This means that the trapping is augmented by the increment in cilia length due to more powerful and effective recovery stokes of cilia within the blood flow.

5.7 Conclusions

Analysis of entropy generation in ciliary induced peristaltic transport of blood with Phan-Thien-Tanner (PTT) non-Newtonian fluid model in a tube under the volumetric concentration of hybrid nanoparticles and internal heat source impacts has been performed in this study. The constituting equations describing the blood flow have been simplified under the postulates of lubrication theory. The resulting equations are solved analytically subject to the prescribed boundary conditions. The alternation in hemodynamic quantities for varying thermophysical parameters has been visualized and illustrated via graphs. Some key consequences of this analysis are pointed out as follows:

- The axial velocity is significantly reduced by boosting Weissenberg number, Phan-Thien-Tanner (PTT) elongation parameter, and cilia length.
- The blood temperature is remarkably augmented with escalating Brinkman number and heat source parameter.
- Impacts of increasing nanoparticle volume fractions have a declining behavior in blood temperature.
- The hybrid nano-blood (Cu- Ag/blood) accomplishes lower temperature via compared to nano-blood (Cu-blood).
- The absolute estimation of the heat transfer coefficient is markedly elevated with ascending Brinkman number, heat source parameter, and nanoparticle volume fractions.
- Larger length of cilia causes a deterioration in the entropy generation number in the blood flow due to cilia movement.
- Bejan number declines with the volumetric concentration of hybrid nanoparticles and it is significantly elevated by heat source.
- Hybrid nano-blood exhibits a greater total entropy number than nano-blood and a contrary behavior is marked in case of Bejan number.
- The trapping of bolus is augmented by the increment in cilia length due to more power and effective recovery stokes of cilia within blood flow.

Acknowledgements The authors are very grateful to anonymous reviewers for their fruitful comments and constructive suggestions to improve our manuscript.

References

Abdelsalam SI, Vafai K (2017) Particulate suspension effect on peristaltically induced unsteady pulsatile flow in a narrow artery: blood flow model. Math Biosci 283:91–105

Abdelsalam SI, Mekheimer KS, Zaher AZ (2020) Alterations in blood stream by electroosmotic forces of hybrid nanofluid through diseased artery: Aneurysmal/stenosed segment. Chin J Phys 67:314–329

Abo-Dahab SM, Abdelhafez MA, Mebarek-Oudina F, Bilal SM (2021) MHD Casson nanofluid flow over nonlinearly heated porous medium in presence of extending surface effect with suction/injection. Indian J Phys 2021. https://doi.org/10.1007/s12648-020-01923-z

Abrar MM, Sagheer M, Hussian S (2020) Thermodynamics analysis of Joule heating and internal heat source over an inclined ciliated tube. Physica A 549:123983

Adesanya SO, Makinde OD (2015) Thermodynamic analysis for a third-grade fluid through a vertical channel with internal heat generation. J Hydrodyn 27:264–272

Agrawal HL, Anawaruddin, (1984) Cilia transport of bio-fluid with variable viscosity. Indian J Pure Appl Math 10:1128–1139

Akbar NS (2015) Entropy generation and energy conversion rate for the peristaltic flow in a tube with magnetic field. Energy 82:23–30

Akbar NS, Butt AW (2014) Heat transfer analysis of viscoelastic fluid flow due to metachronal wave of cilia. Int J Biomathematics 7(6):1450066

Akbar NS, Nadeem S (2012) Peristaltic flow of a Phan-Thien-Tanner nanofluid in a diverging tube. Heat Transf Res 41(1):10–22

Ali A, Banerjee SM, Das S (2021) Hall and ion slip currents impact on magneto-sodium alginate hybrid nanoliquid past a moving vertical plate with ramped heating, velocity slip and Darcy effects. Multidiscip Model Mater Struct 17(1):65–101

Bejan A (1979) A study of entropy generation in fundamental convective heat transfer. J Heat Transf 101:718–725

Bejan A (1982) Second-law analysis in heat transfer and thermal design. Adv Heat Transf 15:1–58

Blake JR (1971) A spherical envelope approach to ciliary propulsion. J Fluid Mech 46(1):199–208

Blake JR (1972) A model for the micro-structure in ciliated organisms. J Fluid Mech 55(1):1–23

Brennen C (1974) Oscillating-boundary layer theory for ciliary propulsion. J Fluid Mech 65:799–824
Bustamante-Marin XM, Ostrowski LE (2017) Cilia and mucociliary clearance. Cold Spring Harb Perspect Biol 4:a028241
Butt AS, Ali A, Munawar S (2013) Slip effects on entropy generation in MHD flow over a stretching surface in the presence of thermal radiation. Int J Exergy 13:1–20
Butt AW, Akbar NS, Mir NA (2020) Heat transfer analysis of peristaltic flow of a Phan-Thien-Tanner fluid model due to metachronal wave of cilia. Biomech Model Mechanobiol 19:1925–1933
Chamkha AJ, Selimefendigil F (2018) MHD free convection and entropy generation in a corrugated cavity filled with a porous medium saturated with nanofluids. Entropy 20:846
Choi SUS (1995) Enhancing thermal conductivity of fluids with nanoparticles. In: Siginer DA, Wang HP(Eds.) Developments and applications of non-Newtonian flows, FED-vol. 231/MD-66, ASME, New York, pp 99-105
Das S, Ali A, Jana RN (2020) Darcian slip flow of rotating magneto-reactive PEG conveying MoS_2 Casson nanofluid with ramped temperature and concentration. Spec Top Rev Porous Media 11:71–102
Drummond IA (2012) Cilia functions in development. Curr Opin Cell Biol 1:24–30
Eddy CA, Pauerstein CJ (1980) Anatomy and physiology of the fallopian tube. Clin Obstet Gynecol 4:1177–1193
El Naby AEHA (2009) Creeping flow of Phan-Thien-Tanner fluids in a peristaltic tube with an infinite long wavelength. J Appl Mech 76(6):064504
Ellahi R, Sait SM, Shehzad N, Ayaz Z (2020) A hybrid investigation on numerical and analytical solutions of electro-magnetohydrodynamics flow of nanofluid through porous media with entropy generation. Int J Numer Method Heat Fluid Flow 30:834–854
Elnaqeeb T, Animasaun IL, Shah MA (2021) Ternary-hybrid nanofluids: significance of suction and dual-stretching on three-dimensional flow of water conveying nanoparticles with various shapes and densities. Zeitschrift Fuür Naturforschung A 76(3):231–243
Fares R, Mebarek-Oudina F, Aissa A, Bilal SM, Öztop HF (2021) Optimal Entropy Generation in Darcy-Forchheimer Magnetized Flow in a Square Enclosure Filled with Silver Based Water Nanoliquid. J Therm Anal Calorim. https://doi.org/10.1007/s10973-020-10518-z
Farooq AA, Siddiqui AM (2017) Mathematical model for the ciliary-induced transport of seminal liquids through the ductuli efferentes. Int J Biomath 10:1750031
Farooq AA, Tripathi D, Elnaqeeb T (2019) On the propulsion of micropolar fluid inside a channel due to ciliary induced metachronal wave. Appl Math Comput 347:225–235
Ghazal S, Makarov JK, de Jonge CJ (2014) Egg transport and fertilization. Glob Libr Women Med 2014. https://doi.org/10.3843/GLOWM.10317
Hanasoge S, Ballard MR, Hesketh PJ, Alexeev A (2017) Asymmetric motion of magnetically actuated artificial cilia. Lab Chip 17:3138–3145
Hayat T, Noreen S, Ali N, Abbasbanday S (2012) Peristaltic motion of Phan-Thien-Tanner fluid in a planar channel. Numer Method Partial Differ Equ 28:737–748
Hayat T, Aslam N, Rafiq M, Alsaedi A (2017) Studying peristaltic transport of shape nanozise silver-water nanoparticles in digestive system with heat generation effect. Int J Heat Mass transf 106:18–24
Husband B, Bu M, Apostolopoulos V, Melvin T, Evans A (2004) Novel actuation of an integrated peristaltic micropump. Microelectron Eng 73:858–863
Ijaz S, Nadeem S (2018) Shape factor and sphericity features examination of Cu and Cu-Al_2O_3 / blood through atherosclerotic artery under the impact of wall characteristic. J Mol Liq 271:361–372
Ijaz S, Iqbal Z, Maraj EN, Nadeem S (2018) Investigate of Cu-CuO / blood mediated transportation in stenosed artery with unique features for theoretical outcomes of hemodynamics. J Mol Liq 254:421–432
Knowles MR, Boucher RC (2002) Mucus clearance as a primary innate defense mechanism for mammalian airways. J Clin Investig 109:571–577
Koriko OK, Adegbie KS, Shah NA, Animasaun IL, Olotu MA (2021) Numerical solutions of the partial differential equations for investigating the significance of partial slip due to lateral velocity and viscous dissipation: The case of blood-gold Carreau nanofluid and dusty fluid. Numer Method Partial Differ Equ 1–29. https://doi.org/10.1002/num.22754
Latham TW (1966) Fluid Motion in a Peristaltic Pump [MS thesis]. Massachusetts Institute of Technology, Cambridge, MA
Lehti MS, Sironen A (2017) Formation and function of sperm tail structures in association with sperm motility defects. Biol Reprod 97:522–536
Makinde OD (2012) Entropy analysis for MHD boundary layer flow and heat transfer over a flat plate with a convective surface boundary condition. Int J Exergy 10:142–154
Makinde OD, Reddy MG, Reddy KV (2017) Effects of thermal radiation on MHD peristaltic motion of Walters-B fluid with heat source and slip conditions. J Appl Fluid Mech 10(4):1105–1112
Marzougui S, Bouabid M, Mebarek-Oudina F, Abu-Hamdeh N, Magherbi M, Ramesh K (2021) A computational analysis of heat transport irreversibility phenomenon in a magnetized porous channel. Int J Numer Method Heat Fluid Flow 31(7):2197–2222
Mehmood OU, Qureshi AA, Yasmin H, Uddin S (2020) Thermo-mechanical analysis of non-Newtonian peristaltic mechanism: modified heat flux model. Phys A Statist Mech Its Appl 550:124014
Mills Z, Aziz B, Alexeev A (2012) Beating synthetic cilia enhance heat transport in microfluidic channels. Soft Matter 45:11508–11513
Munawar S, Saleem N (2020) Entropy analysis of an MHD synthetic cilia assisted transport in a microchannel enclosure with velocity and thermal slippage effects. Coatings 10:414
Munawar S, Saleem N, Aboura K (2016) Second law analysis in the peristaltic flow of variable viscosity fluid. Int J Exergy 20:170–185
Oke AS, Animasaun IL, Mutuku WN, Kimathi M, Shah NA, Saleem S (2021) Significance of Coriolis force, volume fraction, and heat source/sink on the dynamics of water conveying 47 nm alumina nanoparticles over a uniform surface. Chin J Phys 71:716–727
Oliveira PJ, Pinho FT (1999) Analytical solution for fully developed channel and pipe flow of Phan-Thien-Tanner fluids. J Fluid Mech 387:271–280
Pablo JL, DeCaen PG, Clapham DE (2016) Progress in ciliary ion channel physiology. J Gen Physiol 1:37–41
Phan-Thien N, Tanner RI (1977) A new constitutive equation derived from network theory. J. Non-Newtonian Fluid 2(4):353–365
Phan-Thien N, Tanner RI (1978) A nonlinear network viscoelastic model. J Rheol 22(3):259–283
Qiu T, Lee T, Mark AG, Morozov KI, Münster R, Mierka O, Turek S, Leshansky AM, Fischer P (2014) Swimming by reciprocal motion at low Reynolds number. Nat Commun 5:1–8
Rajashekhar C, Mebarek-Oudina F, Vaidya H, Prasad KV, Manjunatha G, Balachandra H (2021) Mass and heat transport impact on the peristaltic flow of Ree-Eyring liquid with variable properties for hemodynamic flow. Heat Transf 2021. https://doi.org/10.1002/htj.22117
Reddy MG, Makinde OD (2016) Magnetohydrodynamic peristaltic transport of Jeffery nanofluid in an asymmetric channel. J Mol Liq 223:1242–1248

Reddy MG, Prasannakumara BC, Makinde OD (2017) Cross diffusion impacts on hydromagnetic radiative peristaltic Carreau-Cassonnanofluids flow in an irregular channel. Defect Diffus Forum 377:62–83

Sadaf H, Iftikhar N, Akbar NS (2019) Physiological fluid flow analysis by means of contraction and expansion with addition of hybrid nanoparticles. Eur Phys J Plus 134:232

Saleem N (2018) Entropy production in peristaltic flow of a space dependent viscosity fluid in asymmetric channel. Therm Sci 22:2909–2918

Saleem N, Munawar S (2020) Entropy analysis in cilia driven pumping flow of hyperbolic tangent fluid with magnetic field effects. Fluid Dyn Res 52:2

Saleem A, Akhtar S, Alharbi FM, Nadeem S, Ghalambaz M, Issakhov A (2020) Physical aspects of peristaltic flow of hybrid nano fluid inside a curved tube having ciliated wall. Res Phys 19:103431

Sarkar J, Ghosh P, Adil A (2015) A review on hybrid nanofluids: recent research, development and applications. Renew Sustain Energy Rev 43:164–177

Shah NA, Animasaun IL, Wakif A, Koriko OK, Sivaraj R, Adegbie KS, Abdelmalek Z, Vaidyaa H, Ijirimoye AF, Prasad KV (2020) Significance of suction and dual stretching on the dynamics of various hybrid nanofluids: Comparative analysis between type I and type II models. Phys Scr 95(9):095205

Shahzadi I, Suleman S, Saleem S, Nadeem S (2020) Utilization of Cu-nanoparticles as medication agent to reduce atherosclerotic lesions of a bifurcated artery having compliant walls. Comput Methods Programs Biomed 184:105–123

Song YQ, Obideyi BD, Shah NA, Animasaun IL, Mahrous YM, Chung JD (2021) Significance of haphazard motion and thermal migration of alumina and copper nanoparticles across the dynamics of water and ethylene glycol on a convectively heated surface. Case Stud Therm Eng 26:101050

Souidi F, Ayachi K, Benyahia N (2009) Entropy generation rate for a peristaltic pump. J Non-Equilib Thermodyn 34:171–194

Sowmya G, Gireesha BJ, Animasaun IL, Shah NA (2021) Significance of buoyancy and Lorentz forces on water-conveying iron(III) oxide and silver nanoparticles in a rectangular cavity mounted with two heated fins: heat transfer analysis. J Therm Anal Calorim 144:2369–2384

Tamada LM, Janet A, Tierney MJ (2002) Keeping watch on glucose. IEEE Spectr 39(4):52–57

Vaidya H, Rajashekhar C, Mebarek-Oudina F, Animasaun IL, Prasad KV, Makinde OD (2021a) Combined effects of homogeneous and heterogeneous reactions on peristalsis of Ree-Eyring liquid: application in hemodynamic flow. Heat Transf 50(3):2592–2609

Vaidya H, Choudhari R, Prasad KV, Khan SU, Mebarek-Oudina F, Patil A, Nagathan P (2021b) Channel flow of MHD Bingham fluid due to peristalsis with multiple chemical reactions: an application to blood flow through narrow arteries. SN Appl Sci 3:186

Vajravelu K, Sreenadh S, Lakshminarayana P, Sucharitha G, Rashidi MM (2016) Peristaltic flow of Phan-Thien-Tanner fluid in an asymmetric channel with porous medium. J Appl Fluid Mech 9:1615–1625

Vajravelu K, Sreenadh S, Dhananjaya S, Lakshminarayana P (2016) Peristaltic flow and heat transfer of a conducing Phan-Thien-Tanner fluid in an asymmetric channel Application to chime movement in small intestine. Int J Appl Mech Eng 21:713–736

Vajravelu K, Radhakrishnamacharya G, Radhakrishnamurty V (2007) Peristaltic flow and heat transfer in a vertical porous annulus with long wave approximation. Int J Nonlinear Mech 42(5):754–759

Wang P, Yuan Y, Xu K, Zhong H, Yang Y, Jin S, Yang K, Qi X (2021) Biological applications of copper-containing materials. Bioact Mater 6:916–927

Wu A, Abbas SZ, Asghar Z, Sun H, Waqas M, Khan WA (2020) A shear-rate-dependent flow generated via magnetically controlled metachronal motion of artificial cilia. Biomech Model Mechanobiol 19:1713–1724

Xu H, Sun Q (2019) Generalized hybrid nanofluid model with the application of fully developed mixed convection flow in a vertical microchannel. Commun Theor Phys 71:903–911

Xu L, Wang YY, Huang J, Chen CY, Wang ZX, Xie H (2020) Silver Nanoparticles: Synthesis, medical applications and biosafety. Theranostics 10:8996–9031